# *IN SITU* OBSERVATIONS OF INNOCULATION AND CRYSTAL GROWTH IN A SYNTHETIC SLAG

C. Orrling, S. Sridhar and A. W. Cramb
Center for Iron and Steelmaking Research,
Carnegie Mellon University
Pittsburgh, PA 15213

**Abstract**

The role of $Al_2O_3$ particles in the initiation of crystallization within a liquid slag was elucidated and quantified through *in situ* observations made by Confocal Scanning Laser Microscopy (CSLM). It was found that at temperatures near the liquidus, blocky crystals precipitated on the surface of the $Al_2O_3$ inclusions the but did not grow with time. At higher undercoolings dendritic and needle-shaped crystals precipitated and grew from the $Al_2O_3$particles. X-ray diffraction was used to determine the precipitated crystalline phases and the results corresponded to the primary phases predicted by the phase diagrams. The observed growth rate of the dendritic were in good agreement with predictions using Ivantsov's model where diffusion in the liquid is controlling growth rate.

**Keywords :** *Confocal Laser Scanning Microscope, slag, inoculation, crystal growth, heterogeneous nucleation, continous castong, mold slag, solidificication, dendrite*

## 1. Introduction

Slags are used in iron and steelmaking processes for a multitude of purposes such as refining and thermal insulation of the molten metal, coverage against re-oxidation of the melt and lubrication between the solid strand and mold in the continuous caster. The performance of the slag depends on the thermo-physical properties that are determined by the polymeric and ionic structural units that comprise the various slags. Slags are also present in an unwanted form as inclusions inside the melt. These are undesirable as they degrade the mechanical properties of the solidified metal.

Crystallization is a property of slags that is of vital importance since it determines the thickness of the solid sag layer in the mold strand gap and this in turn controls the heat transfer in the mold. It is also important in view of inclusions as it is desirable to maintain slag inclusions in a liquid state during rolling and thus it is desirable to suppress crystallization[1,2].

Slag crystallization ha previously been studied through melting, cooling to a known temperature, holding isothermally for a known time, quenching and subsequently examine the formed phases through microscopy [3,4]. Another techniques that has been succesfully applied for studying mold slags is the Double Hot Thermocouple Technique al[5,6].

The crystal growth of binary glass ceramic materials has been studied by a number of different researchers and the crystal growth mechanisms as function of undercooling have been determined[6-10].

In this study the crystallization behavior of synthetic slags (with the addition of alumina particles as innoculants) has been studied *in situ* by the means of the Confocal Laser Scanning Microscope. The objectives of this paper are to study heterogeneous crystallization on fused $Al_2O_3$ particles in synthetic slags.

## 2. Experimental Technique

Confocal scanning laser microscopy (CSLM) combines the advantages of confocal optics and a He-Ne laser and makes it thereby possible to observe samples at high resolution at elevated temperatures. The confocal optics enables the (i) detection of a strong signal from the focal plane while (ii) decreasing the intensity of signals not in the focal plane. By scanning a surface at various focal depths, a 3D image is constructed and thus images of uneven samples can be obtained. The utilization of laser results in high illumination intensity compared to the thermal radiation at elevated temperatures and thus increases the resolution between different phases.

The CLSM system has been used extensively for studying the behavior of inclusions on metallic melts[11)] and solidification and melting behavior[12-13)].

As many slag systems are transparent in the liquid state the crystallization within the melt can be readily studied in the CLSM. The CLSM is well suited for studying the effect of adding solid particles such as alumina, titania, magnesia and zirconia to the melt as innoculants for crystallization. Solid particles are added to the top of the solid slag and immerse in to the melt during melting. The CLSM is focused on a single particle and the temperature is decreased to the experimental temperature where crystallization occurs. In the present experiments the cooling rate was set to 5°C/s.

The slag samples were heated at a heating rate of 15°C/s under a high purity argon atmosphere ($Po_2=10^{-5}$ atm) to a 1420°C and subsequently cooled to the experimental temperature at a cooling rate of 5°C/s. The experimental temperatures were between 1350-1050°C.

The identification of the precipitated crystalline phases was performed by powder X-ray diffraction. The samples for the SEM study and the X-ray diffraction were prepared by using the Double Hot Thermocouple Technique (DHTT) which allows the sample to be quenched at a cooling rate of 300°C/s. The DHTT has been described in detail elsewhere[14].

## 3. Results and Discussion

Three slag samples were studied and their compositions are listed in table 1. The liquidus temperature ($T_L$) and the eutectic temperature ($T_{EUT}$) were determined from the phase diagrams for the present slag systems[15,16)]. It is well known from classical nucleation theory that the onset of crystallization in slags must be a function of cooling rate. To determine the transformation kinetics of crystallization behavior in an undercooled slag one must construct either time temperature transformation (TTT) or continuous cooling transformation (CCT) curves. Figure 1 shows a TTT diagram obtained by the DHTT for the onset crystallization for sample 1. The obtained TTT curve forms a classic C-shape as predicted by classical crystal growth and nucleation theory with the nose position at 1100°C with a minimum incubation time of 60 seconds.

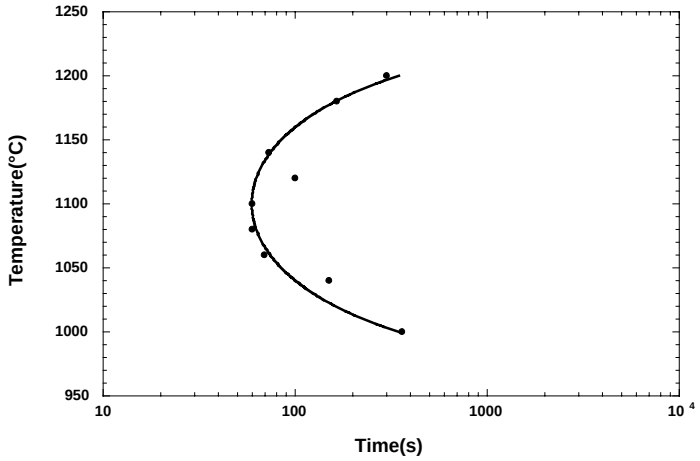


**Figure 1.** TTT diagram for the onset of crystallization of sample 1.

**Table 1.** Slag sample composition

| **Sample** | wt% CaO | wt% $SiO_2$ | wt% $Al_2O_3$ | wt% MgO | $T_L$ | $T_{EUT}$ |
|---|---|---|---|---|---|---|
| 1 | 33.4 | 39.5 | 19.5 | 7.3 | 1330°C[15)] | 1290°C[15)] |
| 2 | 35.7 | 42.51 | 21.2 | 0.4 | 1303°C[16)] | 1264°C[16)] |
| 3 | 39.9 | 40.12 | 20.4 | | 1290°C[16)] | 1264°C[16)] |

### 3.1 Effect of alumina close tro the liquidus temperature

In all experiments performed with the CLSM, the melt remained as an undercooled liquid during cooling to the experimental temperature. The crystals precipitating on the alumina particles close to the liquidus temperature exhibited a cubic morphology and grew as blocks on the alumina particle. The growth of these cubic crystals was limited and stopped after the particle size reached 100 µm in width and height. In the case of Sample 1 the introduction of alumina particles increased the temperature range of crystallization by 150°C compared to crystallization experiments without any alumina particles present in the melt. In addition to increased temperature range the onset of crystallization was almost instantaneous when the samples reached the experimental temperature. Thus, the introduction of the alumina particle in the melt eliminated the potential to under cool the sample.

Some of the cubic crystals detached from the alumina particle and were transported out in the melt as single crystals by convection. An example of a single cubic crystal at 1330°C is shown in Figure 2.

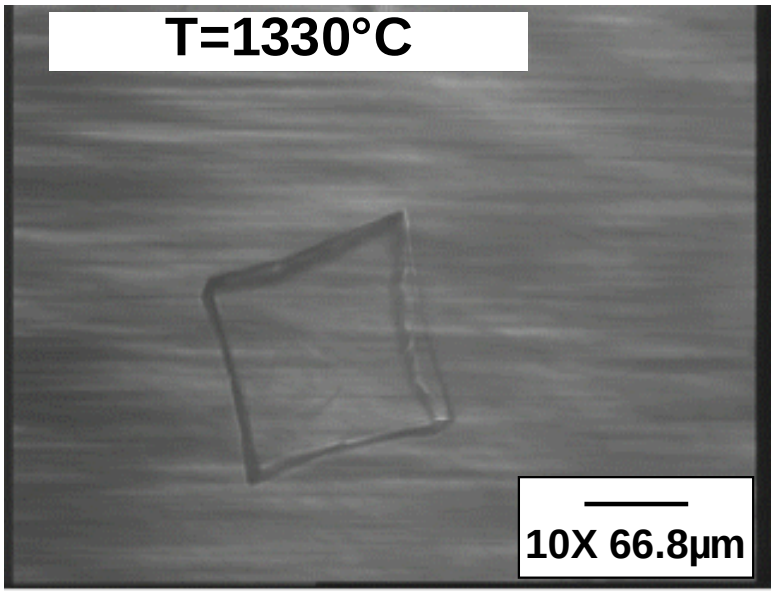


**Figure 2.** Single detached cubic crystal in the melt at 1330°C for sample 1.

The crystal in Figure 3 is fully transparent as the bottom of the platinum pan can be observed through the crystal. Only by the shadows of the edges can the crystal be detected. The size of the crystal in figure 3 remained nearly constant (in 30 seconds it grew less than 1% of its original size).

It is therefore reasonable to assume that the crystal is in equilibrium with the melt. Since these blocky crystals appear at temperatures at and even above the liquidus temperature suggests that they are not thermodynamically stable phases. The phase is formed due to slow dissolution kinetics and reaction between the surface of the alumina particle and the slag. In the cases of Samples 2 and 3 exhibited, in the temperature region close to the liquidus temperature, limited precipitation of blocky crystals similar to that found in sample 1.

### 3.2 Crystal growth in undercooled liquids

As the experimental temperature decreased, the crystal morphology changed from blocky to dendritic crystals for sample 1 and 3. For sample 2 needle shaped crystals were observed between 1250°C and 1100°C and dendritic crystals below 1100°C. At temperatures below $T_{EUT}$ the crystal growth rate become continuous and was only interrupted when crystal arms grew together or reached the walls of the sample holder. The observed crystal morphologies with temperature are summarized in Table 2.

**Table 2.** Crystal morphologies precipitating at different temperatures.

| Morphology | Sample 1 | Sample 2 | Sample 3 |
|---|---|---|---|
| Blocky | 1350°C<T<1275°C | 1300°C<T<1250°C | 1300°C<T<1250°C |
| Needle shaped | | 1250°C<T<1100°C | |
| Dendrites | 1275°C<T<1050°C | 1100°C<T<1050°C | 1250°C<T<1050°C |

The growth of dendritic crystals nucleated on an alumina particle as a function of time at 1237°C is shown in Figure 3.

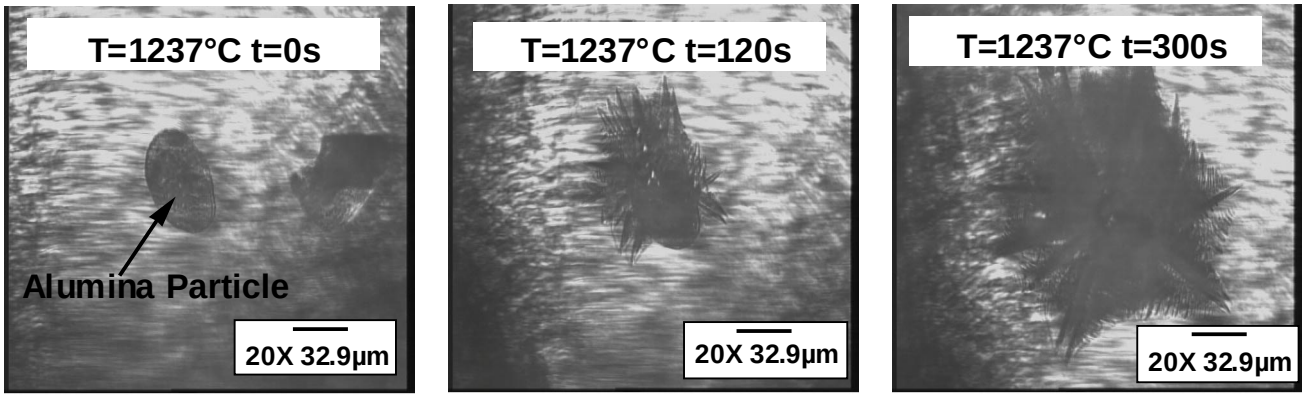


**Figure 3.** Experimental images of dendritic crystals growing out from an $Al_2O_3$ particle at 1237°C in sample 1.

The dendritic structure is easily recognized with the formation of both secondary and tertiary arms. Figure 4 shows needle shaped crystals at 1250°C for sample 2.

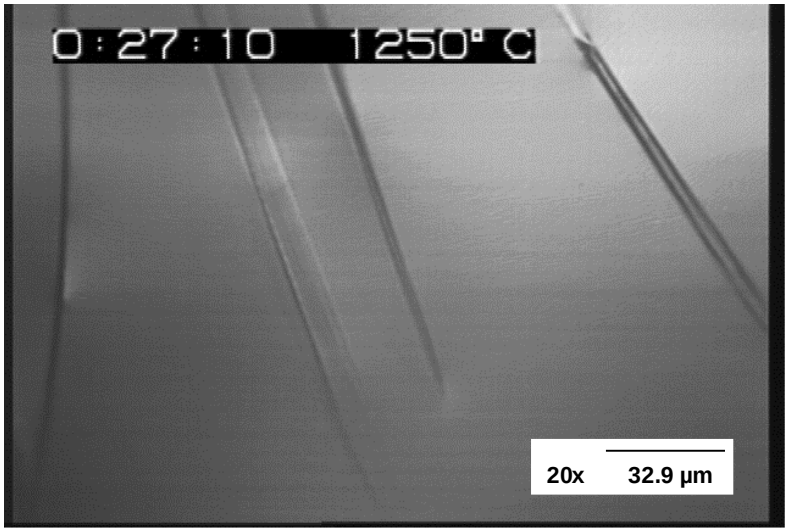


**Figure 4.** Needle shaped crystals growing at 1250°C in sample 2.

Crystal growth was measured by using a computer image analysis program (NIH 1.62) and the crystal sizes and growth rates as a functions of time are shown in Figures 5, 6 and 7 for sample 1, 2 and 3 respectively.

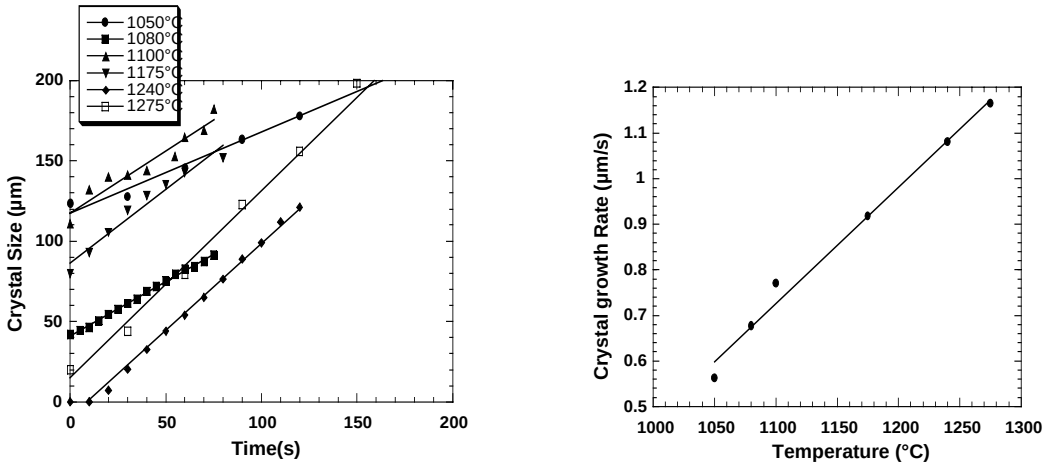


**Figure 5. (a)** Measured crystal growth and **(b)** growth rates for sample 1 at different temperatures.

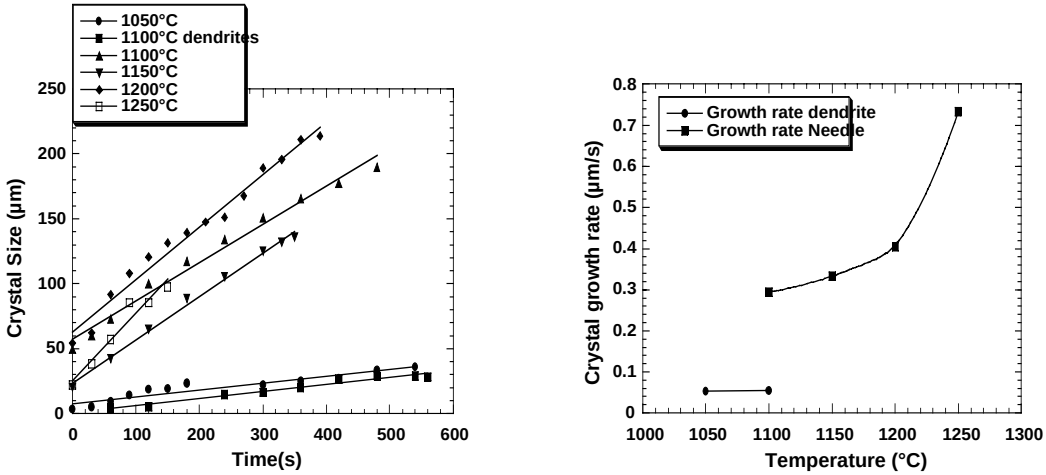


**Figure 6. (a)** Measured crystal growth and **(b)** growth rates for sample 2 at different temperatures.

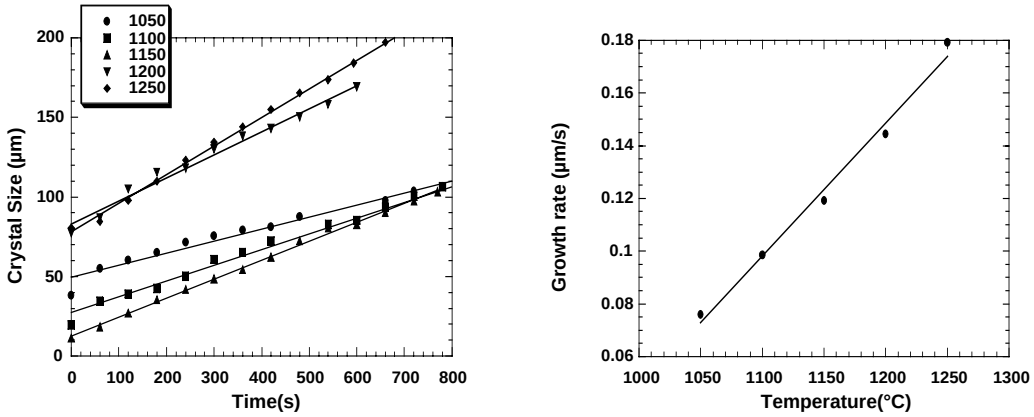


**Figure 7. (a)** Measured crystal growth and **(b)** growth rates for sample 3 at different temperatures.

For sample 1 and 3 the growth rate shows linear temperature dependence but the crystal growth rate for sample 1 is almost ten times that of sample 3. The growth rate for sample 2 shows a more complicated temperature dependence, the growth rate decreases non linearly for the needle shaped crystals and then drops significantly as the crystal morphology transforms to dendritic crystals with decreasing temperature.

The crystal growth rate was found to be linear at a fixed temperature. Therefore, it can be assumed that the growth rate is controlled by a steady state rate of mass transfer through a diffusion layer near the crystal/melt interface. According to the phase diagrams shown in Figure 14, the following can be concluded: (i) the primary phase to precipitate for sample 1 is Melilite ($CaO\text{-}MgO\text{-}SiO_2\text{-}Al_2O_3$) and (ii) in the case of samples 2 and 3 the first phase to precipitate is Anorthite and Gehelenite respectively.

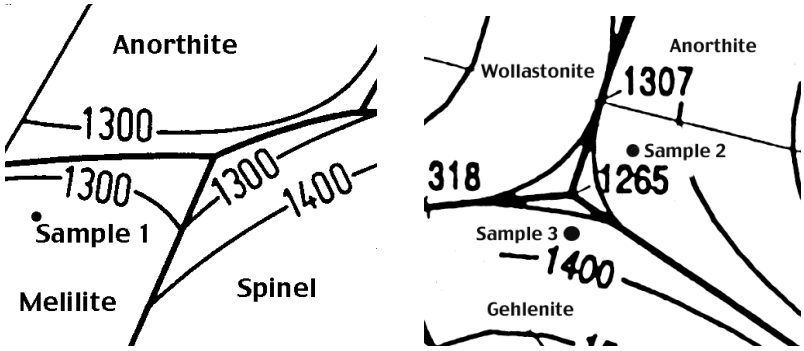


**Figure 8.** Part of phase diagrams showing the position of sample compositions and the eutectics[11].

It is likely that a primary phase is precipitated first and at very long holding times the equilibrium structure is formed. X-ray diffraction was performed on samples quenched from $1150^{O}C$ and the crystalline phases were identified. For sample 1 the crystalline phase was identified as Melilite, for sample 2 it was Anorthite and for sample 3 it was Gehlenite. The results from the X-ray diffraction shows that at 1150°C, the primary phase to precipitate in the undercooled liquid is the same as the primary phase predicted by the

phase diagram from the liquidus surface. The crystallization occurs in these experiments only from a few alumina particles acting as sites for heterogeneous nucleation. The composition of the crystalline phases that were found is summarized in Table 3.

**Table 3.** Composition of the present crystalline phases.

| Crystalline phase | wt% CaO | wt% $SiO_2$ | wt% $Al_2O_3$ | wt% MgO |
|---|---|---|---|---|
| Melilite | 41.02 | 32.97 | 18.64 | 7.37 |
| Anorthite | 20.16 | 43.19 | 36.65 | |
| Gehlenite | 40.90 | 21.91 | 37.18 | |

### 3.3. Comparison between observed and calculated crystal growth rate

A dendrite tip can be described as paraboloid of revulotion and Ivantsov[22] developed a mathematical analysis for the diffusion problem of paraboloid. The following relationship between supersaturation, and dendrite tip radius and growth rate was obtained:

$$\Omega = I(P_C) \tag{3}$$

$$\Omega = \frac{C_l^* - C_0}{C_l^*(1-k)} \tag{4}$$

were k is the partition coefficient ( = $C_l^*$ / $C_s^*$ ) with $C_l^*$ and $C_s^*$ being the concentrations at the interface in the liquid and solid respectively. The Ivantsov function was estimated as:

$$I(P_C) \approx P_C + \frac{P_C}{P_C + 1} \tag{7}$$

$$P_C = \frac{uR}{2D} \tag{8}$$

R=dendrite tip radius

The diffusion coefficient can be estimated with theEyring[18]'s relation:

$$D = \frac{kT}{\eta\lambda} \tag{2}$$

were k is the Boltzmann constant, $\eta$ the viscosity and $\lambda$ the mean interatomic difference (2r). The viscosity data was obtained by using the viscosity model developed at the Department of Metallurgy, Royal Institute of Technology, Stockholm, Sweden[19]. $SiO_2$ was assumed to diffuse as $SiO_4^{4-}$ and, CaO as $Ca^{2+}$ and $Al_2O_3$ as $AlO_3^{3-}$ for the estimation of radius of the diffusing species. The data for ionic radius was taken from Shannon et al[20,21]. For sample 1 and 3 it is assumed that diffusion of ionic silica complex is rate

controlling and for sample 2 the diffusion of alumina ions is rate controlling based on that the biggest complexes would have the lowest mobility and thereby be rate controlling.

Due to limitations in contrast and resolution between the crystal tip and melt, the tip radius could be evaluated only in certain cases for samples 1 and 3 and in no case at all for sample 2. Comparisons between measured values and calculations are shown for these cases in Figures 22 and 23.

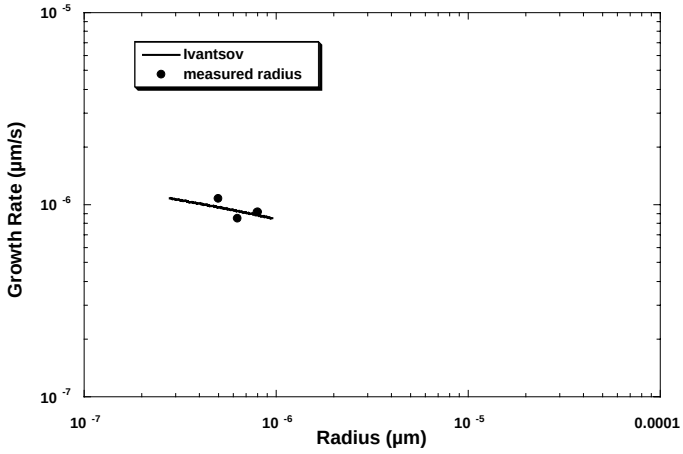


**Figure 22:** Measured and calculated tip radius for sample 1.

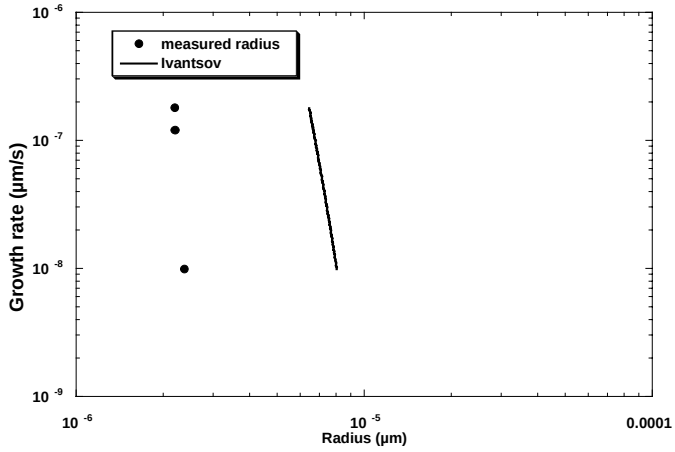


**Figure 23.** Measured and calculated tip radius for sample 3.

While the fit between the calculated values and the measured is very good for sample 1, the calculated ones are three times larger than the measured for sample 3. The discrepancy is however reasonable considering that the rough estimation of the diffusion constant.

The results of this study show that alumina particles act as heterogeneous nucleation sites for slag crystallization. This suggests that un-dissolved inclusions in

mold slags could cause an earlier crystallization than what would be otherwise expected. This would influence both the heat transfer (controlled by the solid slag thickness) and the lubrication that is provided by the liquid slag film.

## 4. Summary

By the means of the CLSM slag crystallization in synthetic slags in the presence of alumina particles was observed *in situ.*

- At temperatures near the liquidus temperature, blocky crystals precipitate on the surface of the alumina particle presumable due to reaction between the particle surface and the slag.
- At highly undercooled conditions, alumina particles act as heterogeneous nucleation sites for precipitation of the primary equilibrium phases as predicted by the phase diagram and eliminate under cooling in these slag systems.
- The growth rate of the crystals was found to fit well with predictions using Ivantsov's solution of the diffusion equation around a parabaloid of revolution.

## 5. Acknowledgment

The authors would like to thank the member companies of the Center for Iron and Steelmaking Research for their financial support. A special thanks goes to Prof. Seetharaman's group at the Department of Metallurgy at Royal Institute of Technology, Stockholm, Sweden for providing the means to calculate the viscosity data.

## 6. References

1. S. Sridhars and A.W. Cramb: Met. and Mat. Trans. B, in press.
2. C.Tse, S. H. Lee, S. Sridhar and A.W. Cramb: Proceedings of the 83rd Steelmakings conference, ISS, Pittsburgh, March 2000, in press.
3. C. Gatellier, H. Gaye, J. Lehmann, J.N. Pontoire, P.V. Riboud: Steel research, Vol.64, 1993, pp.87-92.
4. P. Rocabois, J.N. Pontoire, H. Gaye, J. Lehmann, C. Gatellier: Proceedings of the fifth international conference of clean steel, 2-4 June, 1997, Balatonüred, Hungary, pp. 120-129.
5. C.Orrling, A.Tilliander, Y.Kashiwaya, and A.W.Cramb: Trans. Iron Steel Soc., 27(1), pp.
6. C.Orrling and A.W.Cramb: Met. and Mat. Trans. B, April 2000, in press.
7. P.J. Vergano and D.R. Uhlmann: J.Non-Cryst. Solids, 48 (1982), p.393.
8. P.J. Vergano and D.R. Uhlmann: Phys. Chem. Glasses, 11 (1970), p.39.
9. I Avramov, R. Pascova, B. Samouneva and I. Gutzow: Phys. Chem. Glasses 20, (1979), p.91.
10. L.C. Klein and D.R. Uhlmann: J. Geophys. Res, 79, (1974), p.486.
11. H. Shibata and T. Emi: Materia Japan, 36 (8), (1997), pp. 809-813
12. H. Chikama, H. Shibata, T. Emi and M. Suzuki, Mat. Trans. JIM, 37 (4) (1996), pp. 620-626

13. C. Orrling, Y. Fang, N. Phinichka, S. Sridhar and A. W. Cramb: "Observation and Measurement of Solidification Phenomena at High Temperatures", JOM-e, July (1999), http://www.tms.org/pubs/journals/JOM/9907/Orrling/Orrling-9907.html.
14. Y.Kashiwaya, C.Cicutti, A.W. Cramb, and K.Ishii: ISIJ International, Vol.38,1998, No.4, pp. 348-56.
15. Slag Atlas; 5th ed., Verlag Stahleisen, Düsseldorf, 1995, p.158.
16. G. Eriksson and A.D. Pelton: Metall. Trans. B 24B (1993), pp. 807-15.
17. N.H. Christensen, A.R. Copper, B.S Rawal: J. Am. Ceram. Soc. 56, (1973), p. 557.
18. Slag Atlas; 5th ed., Verlag Stahleisen, Düsseldorf,1995, p.545
19. S. Seetharaman, Du Sichen and J.Y. Zhang: JOM-e, 51(8), 1999, pp. 38-40.
20. R.D. Shannon: Acta. Cryst., B25, (1969), p.925.
21. R.D. Shannon:Acta. Cryst., A32, (1976), p.751.
22. G.P. Ivantsov, Doklady Akademii Nauk SSSR, 58, 1947, p.567.